Piezoelectric Performance and Hydrostatic Parameters of Novel 2–2-Type Composites

Vitaly Yu. Topolov, Christopher R. Bowen, and Andrey V. Krivoruchko

Abstract — **This paper provides a detailed study of the structure - piezoelectric property relationships and the hydrostatic response of 2–2-type composites based on relaxor-ferroelectric $0.72Pb(Mg_{1/3}Nb_{2/3})O_3$–$0.28PbTiO_3$ single crystal material. Type I layers in the composite system are represented by a single-domain [111]-poled single crystal. Changes in the orientation of the crystallographic axes in the Type I layer are undertaken to determine the maximum values of the hydrostatic piezoelectric coefficients d_h^*, g_h^*, and e_h^*, and squared figure of merit $d_h^* g_h^*$ of the composite. The Type II layers are a 0–3 composite whereby inclusions of modified $PbTiO_3$ ceramic are distributed in a polymer matrix. A new effect is described for the first time due to the impact of anisotropic elastic properties of the Type II layers on the hydrostatic piezoelectric response that is coupled with the polarization orientation effect in the Type I layers. Large hydrostatic parameters $g_h^* \approx$ 300–400 mV·m/N, $e_h^* \approx$ 40–45 C/m^2, and $d_h^* g_h^* \sim 10^{-11}$ Pa^{-1} are achieved in the composite based on the $0.72Pb(Mg_{1/3}Nb_{2/3})O_3$–$0.28PbTiO_3$ single crystal. Examples of the large piezoelectric anisotropy ($|d_{33}^*/d_{3f}^*| \geq 5$ or $|g_{33}^*/g_{3f}^*| \geq 5$) are discussed. The hydrostatic parameters of this novel composite system are compared to those of conventional 2–2 piezocomposites.**

Index Terms — **Ferroelectric Materials, Ferroelectric Properties, Piezoelectric and Ferroelectric Transducer Materials**

I. Introduction

Interest in advanced piezo-active composites based on relaxor-ferroelectric single crystals (SCs) [1, 2], such as $(1-x)Pb(Mg_{1/3}Nb_{2/3})O_3 - xPbTiO_3$ (PMN–*x*PT) and $(1-x)Pb(Zn_{1/3}Nb_{2/3})O_3 - xPbTiO_3$, stems from the outstanding electromechanical properties of these SCs near the morphotropic phase boundary [3–5] and associated polarization orientation effects [6] in the composites. These characteristics make them attractive for applications such as sensors, hydropohones, energy-harvesting devices [7–9] and other transducers. Recently, a three-component 2–2-type composite based on the [001]-poled PMN–0.33PT SC was found to exhibit a large hydrostatic piezoelectric response [10]. A promising example of a 2–2-type composite based on a lead zirconate-titanate (PZT) polycrystalline ferroelectric ceramic (FC) was demonstrated in work [11], and the improved performance of this composite was a result of the active role of inclusions in the polymer-containing layers. To date, no comparison of effective parameters of the 2–2-type composites has been carried out for the variety of potential poling directions of the SC components. In addition, the important role of the heterogeneous polymer composite layer and its active component has yet to be studied in detail. The aim of the present paper is to analyze the hydrostatic piezoelectric response and piezoelectric anisotropy of the novel three-component composite based on the [111]-poled SC.

This work was financially supported by the European Research Council under the European Union's Seventh Framework Programme (FP/2007-2013) / ERC Grant Agreement No. 320963 on Novel Energy Materials, Engineering Science and Integrated Systems (NEMESIS) and by the Southern Federal University (research project No. 11.1627.2017/PCh by using the equipment of the Centre of Collective Use 'High Technologies' at the Southern Federal University).

V. Yu. Topolov is with the Department of Physics, Southern Federal University, 344090 Rostov-on-Don, Russia (e-mail: vutopolov@sfedu.ru).

C. R. Bowen is with the Department of Mechanical Engineering, University of Bath, Bath BA2 7AY, UK (e-mail: c.r.bowen@bath.ac.uk).

A. V. Krivoruchko is with the Don State Technical University, 344000 Rostov-on-Don, Russia (e-mail: krivoruchko_av@iivt.donstu.ru).

II. Model Concepts, Effective Properties, and Hydrostatic Parameters

The 2-2-type composite represents a system of parallel-connected layers of two types (Fig. 1) with interfaces that are parallel to the (X_2OX_3) plane, and these layers are regularly arranged along the coordinate OX_1 axis. The *Type I* layers consist of a single-domain SC and are characterized by a spontaneous polarization $\boldsymbol{P}_s^{(1)}$ with an orientation given by the Euler angles φ, ψ, and θ; see inset 1 in Fig. 1. In the present study, we consider a single-domain PMN–*x*PT SC with 3*m* symmetry [5]. To maintain the single-domain state in the SC, an electric bias field can be applied to the sample. At φ = ψ = θ = 0°, the $\boldsymbol{P}_s^{(1)}$ vector is parallel to [111] of the perovskite unit cell, and the crystallographic axes x, y, and z of the SC are oriented as follows: x $\| O X_1^o$, y $\| O X_2^o$, and z $\| O X_3^o$. After a rotation of the crystallographic axes in each Type I layer, conditions x $\| OX_1'$, y $\| OX_2'$, and z $\| OX_3'$ are valid. The transition from $(X_1^o X_2^o X_3^o)$ to $(X_1'X_2'X_3')$ is described by the rotation matrix

$$\| r \| = \begin{pmatrix} \cos\psi\cos\varphi - \sin\psi\cos\theta\cos\varphi & \cos\psi\sin\varphi + \sin\psi\cos\theta\cos\varphi & \sin\psi\sin\theta \\ -\sin\psi\cos\varphi - \cos\psi\cos\theta\sin\varphi & -\sin\psi\sin\varphi + \cos\psi\cos\theta\cos\varphi & \cos\psi\sin\theta \\ \sin\theta\sin\varphi & -\sin\theta\cos\varphi & \cos\theta \end{pmatrix} \quad (1)$$

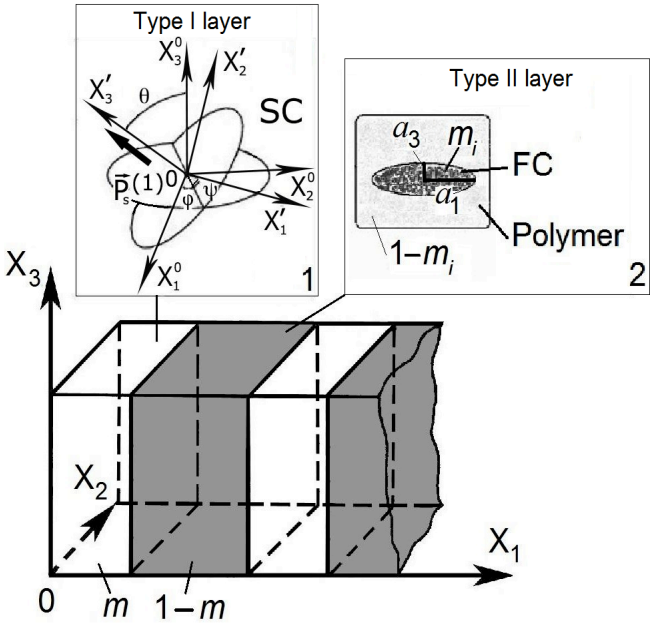

Fig. 1. Schematic of the 2–2-type SC / FC / polymer composite. ($X_1X_2X_3$) is a rectangular coordinate system, m and $1-m$ are volume fractions of the Type I and Type II layers, respectively, m_i is the volume fraction of the FC inclusions in the polymer medium, and $a_1 = a_2$ and a_3 are semi-axes of each inclusion. The Euler angles φ, ψ, and θ characterize the orientation of the crystallographic axes (or spontaneous polarization vector $\boldsymbol{P}_s^{(1)}$) of the SC component.

The *Type II* layer is a FC / polymer medium with 0–3 connectivity in terms of work [12, 13]. The shape of each FC inclusion in the Type II layer (see inset 2 in Fig. 1) obeys the equation $(x_1 / a_1)^2 + (x_2 / a_2)^2 + (x_3 / a_3)^2 = 1$ in the OX_f axes. Hereby $\rho_i = a_1 / a_3 = a_2 / a_3$ is defined as the aspect ratio of the FC inclusion, and m_i is the volume fraction of FC in the Type II layer. It is assumed that the linear sizes of each FC inclusion are much smaller than the thickness of each layer of the composite sample. The FC inclusions occupy sites of a simple tetragonal lattice with unit-cell vectors parallel to the OX_f axes. The composite as a whole (Fig. 1) is described by 2–0–2 connectivity, where the index '2' is related to the SC and the polymer component which is distributed as layers. The index '0' represents the isolated character of the distribution of the FC inclusions in the Type II layers. An alternative formula of the connectivity pattern could be written as 2–2(0–3).

Effective electromechanical properties of the composite that is shown in Fig. 1 are evaluated using three stages as follows. During the first stage, we calculate the full set of electromechanical constants (i.e., elastic compliances $(s_{ab}^E)'$ at electric field E = const, piezoelectric coefficients d_{ij}', and dielectric permittivities $(\varepsilon_{pr}^{\sigma})'$ at mechanical stress σ = const) of the SC in the OX_j' axes. We take into account tensor ranks of the electromechanical constants, $\| r \|$ from Eq. (1), and formulas [6, 14] that enable us to use the matrix (or two-index) form of the aforementioned constants in further evaluations.

In the second stage, the effective properties of the Type II layer, that is the 0–3 FC / polymer composite, are determined by means of the effective field method [6] that takes into consideration an interaction between the FC inclusions. We assume that the components of the 0–3 composite, as shown in inset 2 in Fig. 1, are characterized by elastic moduli $c_{ab}^{(FC),E}$ (FC) and $c_{ab}^{(p),E}$ (polymer), piezoelectric coefficients $e_{ij}^{(FC)}$ and $e_{ij}^{(p)}$ (polymer), and dielectric permittivities $\varepsilon_{qq}^{(FC),\xi}$ (FC) and $\varepsilon_{qq}^{(p),\xi}$ (polymer), where the superscript ξ denotes measurements at constant strain. As a general case, both the FC and polymer components are assumed to be piezoelectric to allow assessment of the potential of using a piezoelectric matrix or inclusions. The effective electromechanical properties of the 0–3 composite are represented in the form of the 9 × 9 matrix as follows:

$$\| C^{(0\text{-}3)} \| = \begin{pmatrix} \| c^{(0-3),E} \| & \| e^{(0-3)} \|^t \\ \| e^{(0-3)} \| & -\| \varepsilon^{(0-3),\xi} \| \end{pmatrix}. \quad (2)$$

In Eq. (2), the superscript t denotes the transposition. Elements of $\| C^{(0\text{-}3)} \|$ from Eq. (2) are found using the formula [6]

$$\| C^{(0\text{-}3)} \| = \| C^{(p)} \| + m_i (\| C^{(FC)} \| - \| C^{(p)} \|)[\| I \| + (1 - m_i) \| S \| \| C^{(p)} \|^{-1} (\| C^{(FC)} \| - \| C^{(p)} \|)]^{-1}. \quad (3)$$

In Eq. (3), $\| C^{(FC)} \|$ and $\| C^{(p)} \|$ are matrices of the electromechanical properties of FC and polymer, respectively, m_i is the volume fraction of FC in the 0–3 composite layer, $\| I \|$ is the identity matrix, and $\| S \|$ is the matrix that contains the Eshelby tensor components [15]. Elements of $\| S \|$ depend on elements of $\| C^{(p)} \|$ and on the aspect ratio ρ_i of the FC inclusion. The averaging procedure based on Eq. (3) is based on the framework of the effective field method [6] which takes into account interactions between the aligned spheroidal FC inclusions in a large polymer medium. The $\| C^{(FC)} \|$ and $\| C^{(p)} \|$ matrices from Eq. (3) have the form similar to that shown in Eq. (2), however in accordance with concepts in [15], the symmetry of the piezoelectric polymer matrix component is ∞mm. If the polymer component is piezo-passive and isotropic, we can simplify the aforementioned formulae as follows: $e_{ij}^{(p)} = 0$, and $\varepsilon_{qq}^{(p),\xi} = \varepsilon_{11}^{(p)} = \varepsilon_{22}^{(p)} = \varepsilon_{33}^{(p)}$.

In the third stage, the effective electromechanical properties of the 2–2-type composite are calculated using the matrix method [6] that allows for the electromechanical interaction between the SC and 0–3 layers (Fig. 1). The electromechanical properties of the composite are characterized by a 9 × 9 matrix

$$\| C^* \| = \begin{pmatrix} \| s^{*E} \| & \| d^* \|^t \\ \| d^* \| & \| \varepsilon^{*\sigma} \| \end{pmatrix}. \quad (4)$$

In Eq. (4), $\| s^{*E} \|$ is the 6 × 6 matrix of elastic compliances at E = const, $\| d^* \|$ is the 6 × 3 matrix of piezoelectric coefficients, $\| \varepsilon^{*\sigma} \|$ is the 3 × 3 matrix of dielectric permittivities of the composite, and the superscript t denotes the transposition. A transition from the matrix elements given for the Type II layer in Eq. (3) to the matrix elements in the form of Eq. (4) is carried out using conventional formulas [14, 16] for the piezoelectric medium. Boundary conditions [6, 7] at the

interface x_1 = const (Fig. 1) imply a continuity of components of mechanical stress σ_{11}, σ_{12} and σ_{13}, strain ξ_{22}, ξ_{23} and ξ_{33}, electric displacement D_1, and electric field E_2 and E_3, i.e., the composite sample is stress-free, and no electric charges are located at the interfaces. The averaging procedure is performed within the framework of the longwave approximation, i.e., when the thickness of the Type I and Type II layers are much smaller than the wavelength of an external field. The matrix $\| M \| = \| \mu_1 \|^{-1} \| \mu_2 \|$ is related to the aforementioned boundary conditions for the interfaces x_1 = const, $\| \mu_1 \|$ is related to the Type I layer, and $\| \mu_2 \|$ is related to the Type II layer. To take into account the full set of electromechanical constants determined on rotation of the $\boldsymbol{P}_s^{(1)}$ vector in each Type I layer, we represent $\| \mu_1 \|$ in the coordinate axes OX_j as follows:

$$\| \mu_1 \| = \begin{pmatrix} 1 & 0 & 0 & 0 & 0 & 0 & 0 & 0 & 0 \\ (s_{12}^E)' & (s_{22}^E)' & (s_{23}^E)' & (s_{24}^E)' & (s_{25}^E)' & (s_{26}^E)' & (d_{12})' & (d_{22})' & (d_{32})' \\ (s_{13}^E)' & (s_{23}^E)' & (s_{33}^E)' & (s_{34}^E)' & (s_{35}^E)' & (s_{36}^E)' & (d_{13})' & (d_{23})' & (d_{33})' \\ (s_{14}^E)' & (s_{24}^E)' & (s_{34}^E)' & (s_{44}^E)' & (s_{45}^E)' & (s_{46}^E)' & (d_{14})' & (d_{24})' & (d_{34})' \\ 0 & 0 & 0 & 1 & 0 & 0 & 0 & 0 & 0 \\ 0 & 0 & 0 & 0 & 1 & 0 & 0 & 0 & 0 \\ (d_{11})' & (d_{12})' & (d_{13})' & (d_{14})' & (d_{15})' & (d_{16})' & (\varepsilon_{11}^\sigma)' & (\varepsilon_{12}^\sigma)' & (\varepsilon_{13}^\sigma)' \\ 0 & 0 & 0 & 0 & 0 & 0 & 0 & 1 & 0 \\ 0 & 0 & 0 & 0 & 0 & 0 & 0 & 0 & 1 \end{pmatrix}. \quad (5)$$

In Eq. (5) we take into account the full set of electromechanical constants of the SC component at fixed values of the Euler angles φ, ψ, and θ, and the lines containing "1" and "0" are related, for instance, to the conditions σ_{11} = const (line 1), E_2 = const (line 8), and E_3 = const (line 9). The $\| \mu_2 \|$ matrix is written in the coordinate axes OX_j as

$$\| \mu_2 \| = \begin{pmatrix} 1 & 0 & 0 & 0 & 0 & 0 & 0 & 0 & 0 \\ s_{12}^{(p),E} & s_{11}^{(p),E} & s_{13}^{(p),E} & 0 & 0 & 0 & 0 & 0 & d_{31}^{(p)} \\ s_{13}^{(p),E} & s_{13}^{(p),E} & s_{33}^{(p),E} & 0 & 0 & 0 & 0 & 0 & d_{33}^{(p)} \\ 1 & 0 & 0 & s_{44}^{(p),E} & 0 & 0 & 0 & d_{15}^{(p)} & 0 \\ 0 & 0 & 0 & 1 & 0 & 0 & 0 & 0 & 0 \\ 0 & 0 & 0 & 0 & 1 & 0 & 0 & 0 & 0 \\ 0 & 0 & 0 & 0 & d_{15}^{(p)} & 0 & \varepsilon_{11}^{(p),\sigma} & 0 & 0 \\ 0 & 0 & 0 & 0 & 0 & 0 & 0 & 1 & 0 \\ 0 & 0 & 0 & 0 & 0 & 0 & 0 & 0 & 1 \end{pmatrix}. \quad (6)$$

Writing Eq. (6), we have taken into account the ∞mm symmetry of the 0–3 composite that contains aligned spheroidal FC inclusions (see inset 2 in Fig. 1) and can determine the full set of electromechanical constants of this composite at fixed values of ρ_i and m_i. By analogy with Eq. (5), we take into account the aforementioned continuity of components of the mechanical and electric fields.

The $\| C^* \|$ matrix of the effective electromechanical properties of the composite is represented in accordance with work [6, 8] as

$$\| C^* \| = [\| C^{(1)} \| \cdot \| M \| m + \| C^{(2)} \| (1 - m)] [\| M \| m + \| I \| (1 - m)]^{-1} \quad (7)$$

and has the structure shown in Eq. (4). In Eq. (7), $\| C^{(1)} \|$ and $\| C^{(2)} \|$ are taken from Eq. (4), $\| M \|$ is expressed in terms of Eqs. (5) and (6), and $\| I \|$ is the identity matrix. While the matrix elements of $\| C^{(1)} \|$ depend on the Euler angles φ, ψ, and θ, and the matrix elements of $\| C^{(2)} \|$ depend on the volume fraction m_i and aspect ratio ρ_i of the FC inclusions, we consider $\| C^* \|$ from Eq. (7) as $\| C^* \| = \| C^*(m, \rho_i, m_i, \varphi, \psi, \theta) \|$. Based on the matrix elements of $\| C^* \|$ from Eq. (7), we obtain the piezoelectric coefficients e_{ij}^* and g_{ij}^* of the composite by using the relations [6, 7, 14] $\| d^* \| = \| e^* \| \cdot \| c^{*E} \|^{-1}$ and $\| g^* \| = \| \varepsilon^{*\sigma} \|^{-1} \cdot \| d^* \|$.

We analyze the following hydrostatic parameters of the 2–2-type composite: firstly, its piezoelectric coefficients

$$d_h^* = d_{33}^* + d_{32}^* + d_{31}^*, \; g_h^* = g_{31}^* + g_{32}^* + g_{33}^*, \text{ and } e_h^* = e_{33}^* + e_{32}^* + e_{31}^*, \quad (8)$$

and, secondly, the squared figure of merit

$$(Q_h^*)^2 = d_h^* g_h^*. \quad (9)$$

Eqs. (8) and (9) are written for a case when the electrodes applied to the composite sample (Fig. 1) are parallel to the (X_1OX_2) plane. The piezoelectric coefficients d_h^*, g_h^*, and e_h^* from Eqs. (8) are used to describe the piezoelectric activity and sensitivity under hydrostatic loading. The squared figure of merit $(Q_h^*)^2$ from Eq. (9) characterizes the sensor signal-to-noise ratio under hydrostatic loading. After taking the piezoelectric items from Eqs. (8) into account, we also analyze the piezoelectric anisotropy of the composite and consider some cases of a large anisotropy of d_{3j}^* and g_{3j}^*.

III. Hydrostatic Piezoelectric Coefficients and Piezoelectric Anisotropy

Among the composite components of interest for further analysis, we consider the [111]-poled PMN–0.28PT SC (Table 1) in the Type I layer, and a modified $PbTiO_3$ FC [18] and polyethylene [7, 19] in the Type II layer. The PMN–0.28PT composition is located in the region of stability of the ferroelectric 3*m* phase at room temperature [5, 20]. In the [111]-poled state, the shear piezoelectric effect concerned with d_{15} strongly dominates over the longitudinal effect: as follows from data in the 2nd column in Table I, $d_{15} / d_{33} \approx 24.6$. For a typical PZT-type FC (see data in the 3rd column in Table I), we have $d_{15} / d_{33} \approx 1.6$. Undoubtedly, the strong shear piezoelectric effect caused by d_{15} can influence the longitudinal and lateral piezoelectric activity of the SC component and the composite as a whole during rotation of the crystallographic axes. We add that the PMN–0.28PT SC is also of interest due to its hydrostatic parameters, see footnotes in Table I. For instance, the value of the piezoelectric coefficient g_h is close to that of the PZT-5 FC, and the e_h value of PMN–0.28PT is negative and in

TABLE I
ROOM-TEMPERATURE ELASTIC COMPLIANCES s_{ab}^E (IN 10^{-12} Pa^{-1}), PIEZOELECTRIC COEFFICIENTS d_{ij} (IN pC / N), AND DIELECTRIC PERMITTIVITY $\varepsilon_{pp}^{\sigma}$ OF POLED PMN–0.28PT SC AND PZT-5 FC

Electromechanical constants	Single-domain [111]-poled PMN–0.28PT SC,[a] 3*m* symmetry [5]	Poled PZT-5 FC,[b] ∞*mm* symmetry [17]
s_{11}^E	8.78	16.3
s_{12}^E	–4.90	–5.67
s_{13}^E	–0.93	–7.17
s_{14}^E	16.87	0
s_{33}^E	6.32	18.7
s_{44}^E	138.69	47.4
s_{66}^E	27.4	43.9
d_{15}	2382	583
d_{22}	–312	0
d_{31}	–43	–170
d_{33}	97	373
$\varepsilon_{11}^{\sigma}/\varepsilon_0$	4983	1730
$\varepsilon_{33}^{\sigma}/\varepsilon_0$	593	1700

[a] Hydrostatic parameters are d_h = 11 pC / N, g_h = 2.10 mV·m / N, e_h = –2.93 C / m^2, and $(Q_h)^2 = 23.1 \cdot 10^{-15}$ Pa^{-1}

[b] Hydrostatic parameters are d_h = 33 pC / N, g_h = 2.19 mV·m / N, e_h = 5.38 C / m^2, and $(Q_h)^2 = 72.3 \cdot 10^{-15}$ Pa^{-1}

terms of the absolute value, about two times smaller than e_h of PZT-5. There is also a large difference between the elastic compliances, s_{12}^E and s_{13}^E, of PMN–0.28PT. The large difference between the dielectric permittivities $\varepsilon_{11}^{\sigma}$ and $\varepsilon_{33}^{\sigma}$ is also typical of PMN–0.28PT SC. These specific examples of the performance of the [111]-poled PMN–0.28PT SC and its symmetry suggest that this piezoelectric component will influence the effective properties of the 2–2-type composite in a different way compared to conventional PZT-type FCs [21].

In the Type II layer, shown in inset 2 of Fig. 1, we vary the volume fraction of the FC m_i and the aspect ratio ρ_i of the FC inclusion to tailor the elastic anisotropy of the 0–3 composite. The differences in the elastic properties of the two types of layers allow control of the dependence of the hydrostatic piezoelectric response of the composite on these elastic properties and their anisotropy. As follows from our evaluations, the Type II layer exhibits a low piezoelectric activity [10] compared to the SC component due to the presence of isolated FC inclusions at $0 < m_i \le 0.3$ and $0.01 \le \rho_i \le 100$. The absolute values of the piezoelectric coefficients of the 0–3 FC / polymer composite are $|d_{3j}^{(0-3)}| < 10$ pC / N [7, 10], even under ideal conditions of electric poling. Hereafter we therefore neglect the lower piezoelectric properties of the Type II layer in the composite and consider only the piezo-active SC component, i.e., the SC at the specific orientation of the crystallographic axes.

In this section, we discuss examples of the hydrostatic piezoelectric response and anisotropy of the piezoelectric properties of the PMN–0.28PT-based composite wherein an 'orientation effect', caused by the rotation of $\boldsymbol{P_s}^{(1)}$ in each SC layer, and the effect of the 0–3 layer on the performance of the composite are considered simultaneously.

A. Achieving High Piezoelectric Coefficients d_h^* and g_h^*

Our analysis of $d_h^*(m, \rho_i, m_i, \varphi, \psi, \theta)$ and $g_h^*(m, \rho_i, m_i, \varphi, \psi, \theta)$ from Eqs. (8) at $0 < m < 1$, $0 < m_i \le 0.3$, and $0.01 \le \rho_i \le 100$ shows that local $\max d_h^* = (d_h^*)_m$ is achieved at moderate volume fractions of SC (i.e., $m \approx 0.3$), and local $\max g_h^* = (g_h^*)_m$ is achieved at small volume fractions of SC (i.e., $0 < m < 0.02$). Such a difference between the volume fractions is due to the strong influence of the dielectric properties of the composite on both g_{3j}^* and g_h^* at $m << 1$, when the Type II layer plays a key role in the dielectric permittivity $\varepsilon_{qr}^{*\sigma}$. We note that for any orientation of the crystallographic axes in the Type I layer (see inset 1 in Fig. 1), the piezoelectric coefficients d_{3j}^* and g_{3j}^* of the composite are linked [14, 16] by the relation

$$d_{3j}^* = \varepsilon_{31}^{*\sigma}\, g_{1j}^* + \varepsilon_{32}^{*\sigma}\, g_{2j}^* + \varepsilon_{33}^{*\sigma}\, g_{3j}^*, \qquad (10)$$

where j = 1, 2, and 3.

By analogy with the 2–0–2 composite based on the domain-engineered [001]-poled SC [10], the value of $\max d_h^*$ of the studied composite increases with increasing ρ_i at m_i = const. This is due to the elastic anisotropy of the Type II layer. According to data from Table II, this anisotropy strongly influences the lateral piezoelectric effect at $\rho_i >> 1$, i.e., in the presence of the heavily oblate FC inclusions in the 0–3 FC / polymer composite (Type II layer). As follows from data for ρ_i = 100 in Table II, the ratio of elastic compliances s_{11} / s_{33} becomes small, and the difference between s_{11} / s_{12} and s_{11} / s_{13} is also relatively small. As a consequence, contributions from

TABLE II
RATIOS OF ELASTIC COMPLIANCES s_{11}/s_{uv} OF THE 0–3 MODIFIED $PbTiO_3$ FC / POLYETHYLENE COMPOSITE WITH SPHEROIDAL INCLUSIONS[a]

ρ_i	m_i	s_{11}/s_{12}	s_{11}/s_{13}	s_{11}/s_{33}
0.01	0.10	–3.95	–69.78	13.5
0.1	0.10	–4.22	–13.2	2.77
1	0.10	–4.86	–4.86	1.00
10	0.10	–5.14	–4.49	0.597
100	0.10	–5.65	–4.54	0.176
100	0.15	–5.67	–4.41	0.126
100	0.20	–5.68	–4.28	0.0998
100	0.25	–5.68	–4.18	0.0831
100	0.30	–5.67	–4.09	0.0709

[a] Elastic moduli c_{ab} of the 0–3 composite are found in accordance with Eq. (3) at the piezoelectric coefficients of FC $e_{ij}^{(FC)} = 0$. The transition from c_{ab} to s_{uv} is carried out in accordance with the relation $\| s \| = \| c \|^{-1}$.

d_{31}^* and d_{32}^* into d_h^* of the composite at $\rho_i = 100$ become small in comparison to $d_{33}^* > 0$, and d_h^* increases. For the PMN–0.28PT-based composite at $\rho_i = 100$ and $m_i = 0.1$, the value of max $d_h^* = 260$ pC / N is achieved at $m = 0.184$, $\varphi = \psi = 0°$, and $\theta = 70°$, and the max d_h^* value is about 23.6 times larger than $d_h = 11$ pC / N of the PMN–0.28PT SC at $\varphi = \psi = \theta = 0°$. The large max d_h^* value of the composite is achieved mainly due to the large piezoelectric coefficient d_{15} of the PMN–0.28PT SC, see the d_{15} value in the 2nd column in Table I. Examples of the volume-fraction (m) behavior of local maxima of hydrostatic parameters at rotation of the crystallographic axes in the Type I layers are shown in Fig. 2.

As follows from our evaluations, max g_h^* and max$[(Q_h^*)_m^2]$ are achieved at small volume fractions of SC ($0 < m < 0.02$, see Fig. 2) irrespective of ρ_i, and local max g_h^* increases with increasing ρ_i at m_i = const. At volume fractions of SC m = 0.10–0.20, the Type II layer (or 0–3 composite) influences g_{3j}^* and g_h^* to a large extent because the inequality $\varepsilon_{33}^{(0-3)} << \varepsilon_{33}^{*\sigma}$ holds at $0 < m_i < 0.4$. It can be seen that changes in the optimal Euler angles, which correspond to local maximum $(g_h^*)_m$ [Fig. 2(a)] or $(Q_h^*)_m^2$ [Fig. 2(b)], are not essential on variations of m. This stability can be due to the presence of the Type II layers that exhibit a large elastic anisotropy (see data in Table II), and at volume fractions of SC $m \le 0.3$. By comparing curves 1 in Fig. 2(a) and (b), one can observe that changes in the piezoelectric coefficients g_{3j}^* from Eqs. (8) on increasing the volume fraction m play an important role in forming the dependence of $(Q_h^*)^2$ from Eq. (9). Despite the monotonic decrease of $(Q_h^*)_m^2$ on increasing m, the $(Q_h^*)_m^2$ values remain large at $m \le 0.3$, see curve 1 in Fig. 2(b).

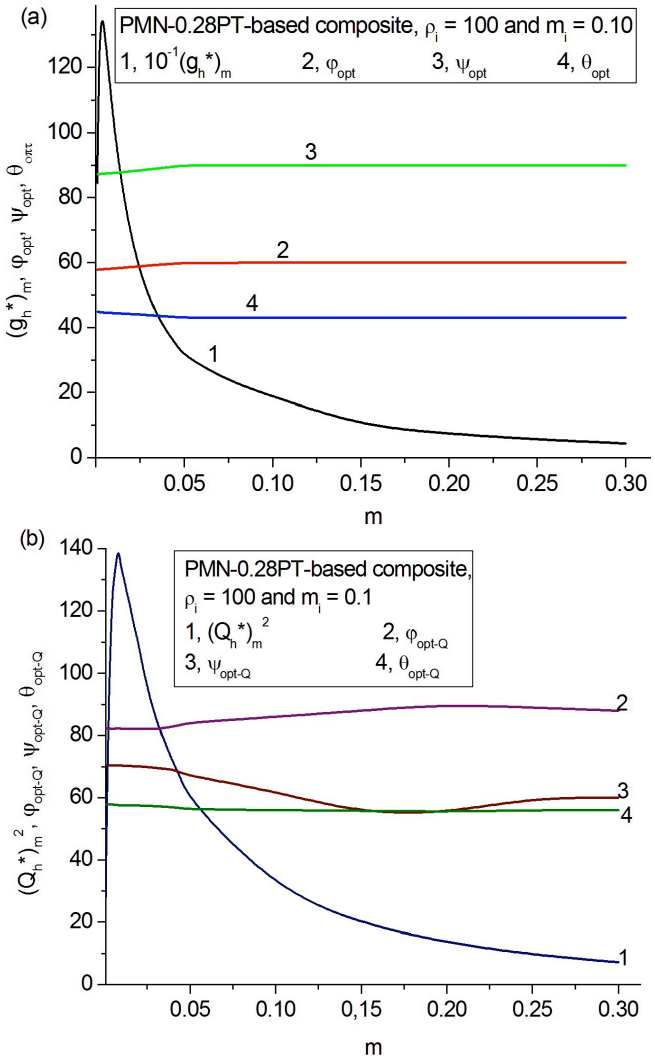

Fig. 2. Local maximum of the hydrostatic piezoelectric coefficient $(g_h^*)_m$ (a, in mV·m / N) and squared figure of merit $(Q_h^*)_m^2$ (b, in 10^{-12} Pa^{-1}) of the 2–2-type PMN–0.28PT SC / modified $PbTiO_3$ FC / polyethylene composite at $0.001 \le m \le 0.3$, $\rho_i = 100$, and $m_i = 0.1$. Curves 2–4 are related to the optimal Euler angles, at which the local maximum of the hydrostatic parameter is achieved.

Our comparison of data in curves 1 in Fig. 2 with data on the 2–2 composites in Table III suggests that the rotation of the crystallographic axes in the Type I layer and the formation of the large elastic anisotropy of the Type II layer clearly leads to large hydrostatic piezoelectric coefficients d_h^* and g_h^* and squared figure of merit $(Q_h^*)^2$. To calculate the hydrostatic parameters of the 2–2 composites, we used Eq. (7) at $m_i = 0$. It is seen from Table III that the values of the hydrostatic parameters evaluated for the 2–2 PZT-5 FC / polyethylene composite by using Eq. (7) are comparable to values obtained for a similar PZT / polymer composite using formulae by Grekov et al. [21] for effective properties. The main reason for any differences between the related parameters of these PZT-based composites is concerned with different polymer components therein. Polyethylene is a softer and more

TABLE III

HYDROSTATIC PIEZOELECTRIC COEFFICIENTS d_h^* (IN PC / N) AND g_h^* (IN mV·m / N) AND SQUARED FIGURE OF MERIT $(Q_h^*)^2$ (IN 10^{-12} Pa^{-1}) OF 2–2 PARALLEL-CONNECTED COMPOSITES

m	Piezoelectric component	Polymer component	d_h^*	g_h^*	$(Q_h^*)^2$
0.05	PMN–0.28PT[a]	Polyethylene	23.5	85.0	2.00
	PZT-5 FC	Polyethylene	79.6	113	9.03
	PZT FC	Polymer	57.8[b]	76.3[b]	4.41[b]
	PMN–0.28PT[c]	Polyethylene	128[d]	164[e]	16.1[f]
0.10	PMN–0.28PT[a]	Polyethylene	24.0	44.5	1.06
	PZT-5 FC	Polyethylene	84.8	58.6	4.97
	PZT FC	Polymer	59.5[b]	39.4[b]	2.35[b]
	PMN–0.28PT[c]	Polyethylene	128[d]	83.2[e]	5.57[f]

[a] [111]-poled SC at the Euler angles $\varphi = \psi = \theta = 0°$, see inset 1 in Fig. 1

[b] Results from work [21]

[c] [111]-poled SC at the Euler angles φ. ψ, and θ which are related to local maximum of one of the hydrostatic parameters

[d] Local max d_h^* at $\varphi = 60°$, $\psi = 90°$, and $\theta = 71°$

[e] Local max g_h^* at $\varphi = 60°$, $\psi = 90°$, and $\theta = 46°$

[f] Local max$[(Q_h^*)^2]$ at $\varphi = 0°$, $\psi = 90°$, and $\theta = 119°$

compliant component in comparison to polymer from work [21], and this enables us to achieve larger values of d_h^*, g_h^*, and $(Q_h^*)^2$ at m = const. A considerable increase of the aforementioned hydrostatic parameters of the PMN–0.28PT SC / polyethylene composite is observed on rotation of the crystallographic axes in the Type I layer. Even at a relatively small volume fraction of SC $m = 0.05$, it is possible to achieve an increase of d_h^* g_h^*, and $(Q_h^*)^2$ by about 5.4, 1.9, and 8 times, respectively, in comparison to the same composite at Euler angles $\varphi = \psi = \theta = 0°$, see Table III. However, the hydrostatic parameters remain lower than local maxima of these parameters of the related 2–2-type composite at $0.05 \le m < 0.15$, $\rho_i = 100$, and $m_i = 0.1$ [see, e.g. curves 1 in Fig. 2(a) and (b)]. It is also seen from Table III that the hydrostatic parameters d_h^* g_h^*, and $(Q_h^*)^2$ of the 2–2 PZT-based composites are smaller than the similar parameters of the 2–2 PMN–0.28PT SC / polyethylene composite wherein rotation of the crystallographic axes is implemented. Values of local maxima of g_h^* and $(Q_h^*)^2$ of the 2–0–2 composite (Fig. 2) are larger than values of g_h^* and $(Q_h^*)^2$ of the 2–2 PZT-based composites, and this advantage of the latter composites is mainly due to the 'orientation effect' in the 2–0–2 composite.

B. Achieving Large Piezoelectric Anisotropy

The problem of the large piezoelectric anisotropy is of independent interest due to potential piezoelectric energy-harvesting applications [7] and due to the presence of the modified $PbTiO_3$ FC in the Type II layer. Due to the rotation of the main crystallographic axes in the Type I layer and Eq. (10), differences in the anisotropy of d_{3j}^* and g_{3j}^* are observed in the studied 2–0–2 composite based on the [111]-poled PMN–0.28PT SC. Hereafter we consider examples of validity of conditions

$$|d_{33}^* / d_{3f}^*| \ge 5 \qquad (11)$$

and

$$|g_{33}^* / g_{3f}^*| \ge 5, \qquad (12)$$

where $f = 1$ and 2. To show the important role of the Type II layer in forming the large piezoelectric anisotropy and to achieve a relatively large piezoelectric sensitivity, we assume that the volume fraction of SC in the composite is $m = 0.1$.

The PMN–0.28PT-based composite is characterized by relatively narrow regions of Euler angles [Fig. 3(a) and (b)] where conditions (11) and (12) hold. This circumstance is to be taken into account at the preparation of the SC cuts with the relevant orientation of the crystallographic axes. Of specific interest is the point related to $\psi = 0°$ and $\theta = 90°$ in Fig. 3(a) and (b). At $\varphi = \psi = 0°$ and $\theta = 90°$, high ratios $|d_{33}^* / d_{31}^*| = 6.96$, $|d_{33}^* / d_{32}^*| = 358$, $|g_{33}^* / g_{31}^*| = 6.99$, and $|g_{33}^* / g_{32}^*| = 200$ are achieved at $d_{33}^* = 210$ pC / N and $g_{33}^* = 67.1$ mV·m / N. At

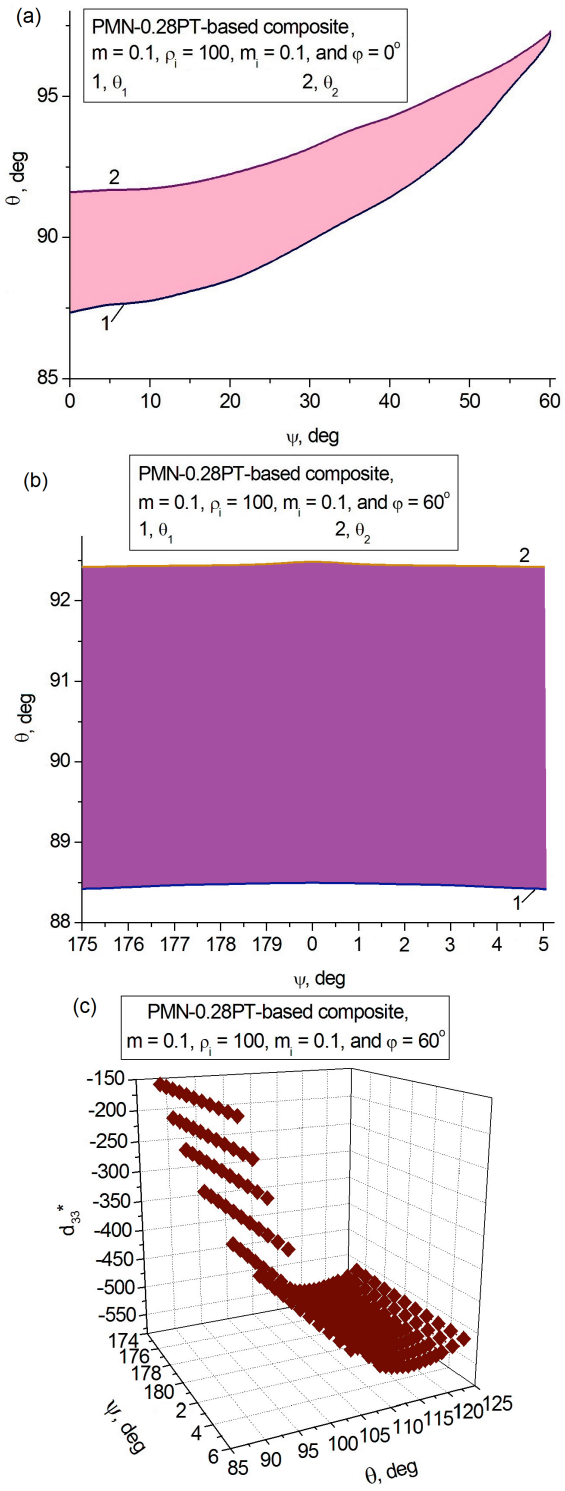

Fig. 3. Regions of the large piezoelectric anisotropy of piezoelectric coefficients d_{3j}^* (a) and g_{3j}^* (b) and behavior of the piezoelectric coefficient d_{33}^* near local minimum (c, in pC / N) in the 2–2-type PMN–0.28PT SC / modified $PbTiO_3$ FC / polyethylene composite. The Euler angles θ_k in graphs (a) and (b) are related to the bounds of validity of conditions (11) and (12), respectively.

small deviations from $\psi = 0°$, we obtain $|d_{33}^* / d_{31}^*| = 6.97$, $|d_{33}^* / d_{32}^*| = 330$, $|g_{33}^* / g_{31}^*| = 7.00$, and $|g_{33}^* / g_{32}^*| = 190$ (at $\psi = 1°$), $d_{33}^* / d_{31}^*| = 6.98$, $|d_{33}^* / d_{32}^*| = 267$, $|g_{33}^* / g_{31}^*| = 7.01$, and

$|g_{33}^*/g_{32}^*| = 166$ (at $\psi = 2°$), etc. The similar set of ratios $|d_{33}^*/d_{31}^*| = 6.96$, $|d_{33}^*/d_{32}^*| = 358$, $|g_{33}^*/g_{31}^*| = 6.99$, and $|g_{33}^*/g_{32}^*| = 200$ is related to the Euler angles $\varphi = 60°$, $\psi = 0°$, and $\theta = 90°$, and the composite at such an orientation of the crystallographic axes and at $m = 0.1$ is characterized by piezoelectric coefficients $d_{33}^* = -210$ pC / N and $g_{33}^* = -67.1$ mV·m / N. As follows from our evaluations, $\min d_{33}^*$ and the largest $|d_{33}^*|$ value are achieved with an Euler angle θ that differs from the θ_k angles in Fig. 3(a) by a few tens of degrees, and therefore, the condition (11) holds for the composite at $|d_{33}^*| \sim 10^2$ pC / N. Such a feature of the piezoelectric activity of the composite enables us to choose the Euler angle θ from a wider range than that shown in Fig. 3(a) and to avoid a drastic decrease of $|d_{33}^*|$. The larger values of $|d_{33}^*|$ at the valid condition (11) imply advantages of the studied PMN–0.28PT-based composite over the $PbTiO_3$-type FCs with a large piezoelectric anisotropy [18, 22].

C. Achieving High Piezoelectric Coefficient e_h^*

The volume-fraction (m) behavior of the hydrostatic piezoelectric coefficient e_h^* from Eqs. (8) strongly differs from the volume-fraction behavior of d_h^* and g_h^*. A maximum value of e_h^* in the 2–2-type composites is achieved at a large volume fraction of SC m; as a rule [6, 7], at $m > 0.7$. This is a result of the complex combination of the piezoelectric and elastic properties at the polarization orientation effect. In the PMN–0.28PT-based composite analyzed in this paper, we observe a new influence of the elastic properties of the Type II layer on e_h^*. Firstly, a larger value of e_h^* at the maximum point is achieved in the presence of FC inclusions with $\rho_i << 1$ and m_i = const. Secondly, the optimal volume fraction m_{opt} related to $\max e_h^*$ undergoes minor changes at $\rho_i = 0.01$–100 and m_i = const. Thirdly, large e_h^* values (Fig. 4) are achieved in the composite despite the negative value of $e_h = -2.93$ C / m^2 in the single-domain PMN–0.28PT SC at $\varphi = \psi = \theta = 0°$. To the best of our knowledge, no similar volume-fraction and orientation behavior was earlier considered in papers on piezo-active composites. Fig. 4 shows that changes in the Euler angle θ influence e_h^* to a large degree. Such a behavior is a result of the orientation of the spontaneous polarization vector $\boldsymbol{P}_s^{(1)}$ with respect to the OX_3 axis (Fig. 1). Replacing the Type II layer at $\rho_i = 0.01$ and $m_i = 0.1$ with the related layer at ρ_i = 100 and $m_i = 0.1$ leads to a decrease of $\max e_h^*$. According to our data on the PMN–0.28PT-based composite at $\rho_i = 100$ and $m_i = 0.1$, $\max e_h^* = 41.5$ C / m^2 is achieved at $m = 0.830$.

The considerable difference between $e_h < 0$ of the SC component and $\max e_h^* > 0$ in the composite is due to an appreciable polarization orientation effect in the Type I layer and the large elastic anisotropy of the Type II layer. It is impossible to extract the role of each effect, but it is obvious that the elastic anisotropy in the Type II layer becomes important even at small volume fractions of FC inclusions, e.g. at $m_i = 0.1$. Absolute values of ratios of elastic compliances $|s_{11}/s_{q3}| >> 1$ (q = 1 and 3) in the Type II layer at $\rho_i = 0.01$ (see Table II) lead to a considerable redistribution of internal elastic and electric fields in the sample and correspondingly to large values of e_{33}^*.

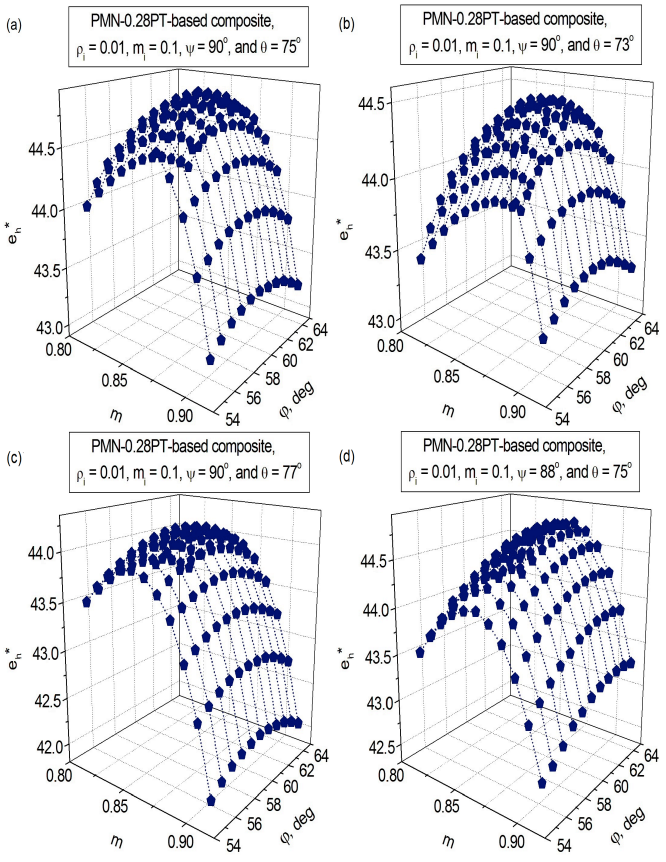

Fig. 4. Behavior of the hydrostatic piezoelectric coefficient e_h^* (in C / m^2) near the maximum point in the 2–0–2 PMN–0.28PT SC / modified $PbTiO_3$ FC / polyethylene composite at $\rho_i = 0.01$ and $m_i = 0.1$.

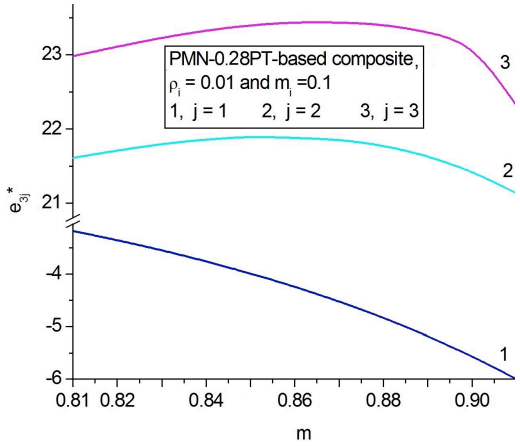

Fig. 5. Contributions from the piezoelectric coefficients e_{3j}^* (in C / m^2) into e_h^* near its maximum point in the 2–2-type PMN–0.28PT SC / modified $PbTiO_3$ FC / polyethylene composite at $\rho_i = 0.01$ and $m_i = 0.1$.

The considerable difference between $e_h < 0$ of the SC component and $\max e_h^* > 0$ in the composite is due to the

important role of the elastic properties of the composite in the formation of the piezoelectric coefficients e_{3j}^*. Fig. 5 shows that in the vicinity of $\max e_h^*$, a more favorable behavior of $e_{3j}^* > 0$ is observed. Due to the orientation effect, the condition $e_{33}^* \approx e_{32}^*$ holds (see curves 2 and 3 in Fig. 5) that leads to 40 C / m^2 < e_h^* < 45 C / m^2.We add for comparison that the 2–2 PMN–0.28PT SC / polyethylene composite at $\varphi = \psi = \theta = 0°$ is characterized by $\max e_h^*$ = 8.77 C / m^2, and this maximum is achieved at m = 0.924. For the 2–2 PZT-5 FC / polyethylene composite, $\max e_h^*$ = 15.1 C / m^2 is related to the volume fraction of FC m = 0.943. The smaller volume fractions of SC m and larger values of e_h^* in Fig. 4 highlight the obvious advantage of the 2–0–2 PMN–0.28PT-based composite over other known 2–2-type piezocomposites [1, 6, 7, 13].

D. Large Effective Parameters and Potential Applications of the PMN–0.28PT-Based Composite

The studied 2–2-type composite is of interest due to the orientation effect in the Type I layer and the considerable anisotropy of elastic properties in the Type II layer. The value of $\max e_h^* \approx$ 45 C / m^2 (Fig. 4) is approximately 3–8.5 times larger than e_h of commonly available poled FCs with a perovskite-type structure [17, 18, 22]. The large e_h^*, e_{32}^*, and e_{33}^* values are achieved at large volume fractions of SC $m \approx$ 0.8 (Figs. 4 and 5), where the orientation effect plays a dominating role. The $(Q_h^*)_m{}^2$ values related to the studied 2–0–2 composite at 0.05 < $m \le$ 0.1 [see curve 1 in Fig. 2(b)] are about 1.5–2 times larger than $(Q_h^*)^2$ of oriented 2–2 and 3–3 PZT FC / polymer composites [13]. Conditions (11) and (12) for large piezoelectric anisotropy are valid with relatively large piezoelectric coefficient $|d_{33}^*|$, see Fig. 3(c), that provides a considerable electromechanical coupling for the longitudinal piezoelectric effect.

The set of the hydrostatic parameters of the studied 2–2-type composite makes it attractive for hydroacoustic and related applications. Valid conditions (11) and (12) along with a considerable longitudinal piezoelectric effect suggest that such a composite may be of value in sensor, transducer and related energy-harvesting applications. In general, a successful combination of the orientation effect and elastic anisotropy can lead to new important results concerned with the piezoelectric performance, electromechanical coupling and hydrostatic response of these fascinating composite systems.

The manufacture of the 2–2-type SC / FC / polymer composite can be carried out as a series of stages. As is known, SC-based 2–2 composites are often fabricated using the dice and fill method where a SC plate is diced along the required crystallographic direction. An orientation of the crystallographic axes in each SC Type I layer is selected in advance, by taking into account the maximum value of the specific hydrostatic parameter required (see, e.g. data in Figs. 2 and 4). The width of the SC Type I layer would be limited by processing limitations, such as a blade vibration [23, 24]. After dicing, the grooves can be filled with the Type II polymer matrix, using a vacuum [23], and FC inclusions within a polymer matrix could be aligned within the matrix using dielectrophoretic assembly prior to curing to engineer anisotropy into a composite material. This process has been used for FC inclusions and also high aspect-ratio particulates [25, 26]; moreover, a simultaneous combination of dielectrophoresis and poling has also been achieved [26].

IV. Conclusion

We have studied a novel 2–2-type SC / FC / polymer composite structure shown in Fig. 1, the set of relevant hydrostatic parameters of the composite based on the [111]-poled PMN–0.28PT SC, and conditions (11) and (12) for the large piezoelectric anisotropy. Two main new features are reported for the description of the piezoelectric performance of the studied composite. First, we have used components with contrasting properties: for instance, the [111]-poled SC with the strong shear piezoelectric effect (see data on d_{15} in the 2nd column of Table I), FC, and polymer. Second, the polarization orientation effect in the SC layer leads to the high piezoelectric performance, and the elastically anisotropic 0–3 layer (see data in Table II) can effectively influence the piezoelectric anisotropy and hydrostatic response of the composite as a whole. The piezoelectric activity of the SC layer and the important role of the elastic subsystem of the 0–3 layer lead to large hydrostatic parameters in specific ranges of the volume fractions m and m_i, aspect ratios ρ_i, and Euler angles φ, ψ, and θ. Maximum values of the hydrostatic parameters of the studied 2–2-type composite, as shown in Figs. 2 and 4, are by two–three orders-of-magnitude larger than the related parameters of the single-domain PMN–0.28PT SC. It is shown that the hydrostatic parameters of the 2–2-type composite are larger than the similar parameters of the 2–2 PZT-based composites from Table III, and the main reason for the large parameters is concerned with rotation of the crystallographic axes in the SC layers.

The 0–3 layer also plays an important role in forming the large piezoelectric coefficient e_h^* and in achieving the large piezoelectric anisotropy. Due to the ability to attain $d_{33}^* \sim 10^2$ pC / N at a relatively small volume fraction of SC m = 0.1, we put forward the 2–2-type composite that obeys conditions (11) and (12) and has obvious advantages over the anisotropic FCs based on $PbTiO_3$ [18, 22]. The sets of the large hydrostatic parameters and the large piezoelectric anisotropy (Section III) have not been previously reported for other two- or three-component composites based on relaxor-ferroelectric SCs. The large values of the parameters of the studied composite make them important for hydroacoustic, acoustic antenna, transducer, sensor, and energy-harvesting applications.

References

[1] S. Zhang and F. Li, "High performance ferroelectric relaxor-$PbTiO_3$ single crystals: Status and perspective", *J. Appl. Phys*., vol. 111, no. 3, p. 031301-50 p., Feb. 2012.

[2] S. Zhang, F. Li, J. Luo, R. Sahul, and T. R. Shrout, "Relaxor-$PbTiO_3$ single crystals for various applications", *IEEE Trans. Ultrason., Ferroelectr., a. Freq. Control*, vol. 60, no. 8 , pp.1572–1580, Aug. 2013.

[3] R. Zhang, B. Jiang, and W. Cao, "Elastic, piezoelectric, and dielectric properties of multidomain $0.67Pb(Mg_{1/3}Nb_{2/3})O_3$–$0.33PbTiO_3$", *J. Appl. Phys*., vol. 90, no. 7, pp.3471–3475, Oct. 2001.

[4] R. Zhang, B. Jiang, W. Jiang, and W. Cao, "Complete set of elastic, dielectric, and piezoelectric coefficients of $0.93Pb(Zn_{1/3}Nb_{2/3})O_3$ – $0.07PbTiO_3$ single crystals poled along [001]". *Appl. Phys. Lett.* Vol. 89, no. 24, p. 242908–3 p., Dec. 2006.

[5] G. Liu, W. Jiang, J. Zhu, and W. Cao, "Electromechanical properties and anisotropy of single- and multi-domain $0.72Pb(Mg_{1/3}Nb_{2/3})O_3$-$0.28PbTiO_3$ single crystals", *Appl. Phys. Lett*., vol. 99, no. 16, p. 162901-3 p., Oct. 2011.

[6] V. Yu. Topolov, P. Bisegna, and C. R. Bowen, *Piezo-Active Composites. Orientation Effects and Anisotropy Factors*. Heidelberg: Springer, 2014.

[7] C. R. Bowen, V. Yu. Topolov, and H. A. Kim, *Modern Piezoelectric Energy-Harvesting Materials*. Switzerland: Springer, 2016.

[8] C. R. Bowen, V. Yu. Topolov, A. N. Isaeva, and P. Bisegna, "Advanced composites based on relaxor-ferroelectric single crystals: from electromechanical coupling to energy-harvesting applications", *CrystEngComm*, vol. 18, no. 32, pp. 5986–6001, Aug. 2016.

[9] Z. Zeng, L. Gai, X. Wang, D. Lin, S. Wang, H. Luo, and D. Wang, "A plastic-composite-plastic structure high performance flexible energy harvester based on PIN-PMN-PT single crystal/epoxy 2-2 composite", *Appl. Phys. Lett*., vol. 110, p. 103501-5 p., Mar. 2017.

[10] V. Yu. Topolov, C. R. Bowen, and I. A. Ermakov, "Remarkable hydrostatic piezoelectric response of novel 2–0–2 composites", *Ferroelectrics. Lett. Sec*., vol. 43, nos. 4-6, pp.90–-95, Sep. 2016.

[11] X. Dongyu, C. Xin, and H. Shifeng, "Investigation of inorganic fillers on properties of 2–2 connectivity cement / polymer based piezoelectric composites", *Constr. Build. Mater*., vol. 94, pp. 678–683, Sep. 2015.

[12] R. E. Newnham, D. P. Skinner, and L. E. Cross, "Connectivity and piezoelectric – pyroelectric composites", *Mater. Res. Bull*., vol. 13, no. 5, pp. 525–536, May 1978.

[13] E. K. Akdogan, M. Allahverdi, and A. Safari, "Piezoelectric composites for sensor and actuator applications", *IEEE Trans. Ultrason., Ferroelectr., a. Freq. Control*, vol. 52, no. 5, pp. 746–775, May 2005.

[14] I. S. Zheludev, *Physics of Crystalline Dielectrics. Vol. 2. Electrical Properties*. New York: Plenum, 1971.

[15] J. H. Huang and W.-S. Kuo, "Micromechanics determination of the effective properties of piezoelectric composites containing spatially oriented short fibers", *Acta Mater*., vol. 44, no. 12, pp. 4889–4898, Dec. 1996.

[16] T. Ikeda, *Fundamentals of Piezoelectricity*. Oxford: Oxford University Press, 1990.

[17] D. A. Berlincourt, D. R. Cerran, and H. Jaffe, "Piezoelectric and piezomagnetic materials and their function in transducers". W. Mason (ed.) *Physical Acoustics. Principles and Methods.* Vol. 1*: Methods and Devices.* Pt A. New York, London: Academic Press, 1964, pp. 169–270.

[18] S. Ikegami, I. Ueda, and T. Nagata, "Electromechanical properties of $PbTiO_3$ ceramics containing La and Mn", *J. Acoust. Soc. Am*., vol. 50, no. 4, pt 1, pp.1060–1066, Apr. 1971.

[19] K. E. Evans and K. L. Alderson, "The static and dynamic moduli of auxetic microporous polyethylene", *J. Mater. Sci. Lett*., vol. 11, no. 24, pp.1721–1724, Dec. 1992.

[20] V. A. Shuvaeva, A M Glazer, and D Zekria, "The macroscopic symmetry of $Pb(Mg_{1/3}Nb_{2/3})_{1-x}Ti_xO_3$ in the morphotropic phase boundary region (x = 0.25 – 0.5)", *J. Phys.: Condens. Matter*, vol. 17, no. 37, pp. 5709–5723, Sep. 2005.

[21] A. A. Grekov, S. O. Kramarov, and A. A. Kuprienko, "Anomalous behavior of the two-phase lamellar piezoelectric texture", *Ferroelectrics*, vol. 76, pp. 43–48, Nov. 1987.

[22] Y. Xu, *Ferroelectric Materials and Their Applications*. Amsterdam: North-Holland, 1991.

[23] W. Wang, S. W. Or, Q. Yue, Y. Zhang, J. Jiao, C. M. Leung, X. Zhao, and H. Luo, "Ternary piezoelectric single-crystal PIMNT based 2-2 composite for ultrasonic transducer applications", *Sensors and Actuators A: Physical*, vol. 196, no. 1, pp. 70–77, Jul. 2013.

[24] L. Li, S. Zhang, Z. Xu, X. Geng, F. Wen, J. Luo, and T. R. Shrout, "Hydrostatic piezoelectric properties of [011] poled $Pb(Mg_{1/3}Nb_{2/3})O_3$-$PbTiO_3$ single crystals and 2-2 lamellar composites", *Appl. Phys. Lett*., vol. 104, no. 3, p.032909 – 5 p., Jan. 2014.

[25] D. A. van den Ende, H. J. van de Wiel, W. A. Groen, and S. van der Zwaag, "Direct strain energy harvesting in automobile tires using piezoelectric PZT–polymer composites", *Smart Mater. Struct.*, vol. 21, no. 1, 015011 – 11 p., Jan. 2012.

[26] H Khanbareh, S van der Zwaag, and WA Groen, "In-situ poling and structurization of piezoelectric particulate composites", J. Intel. Mater. Syst. Struct., Feb. 2017, DOI: 10.1177/1045389X17689928

Vitaly Yu. Topolov was born in Rostov-on-Don (USSR, now Russia) on November 8th, 1961. He received the qualification "Physicist. Educator" (honours degree, 1984) and degrees "Candidate of Sciences (Physics and Mathematics)" (1987) and "Doctor of Sciences (Physics and Mathematics)" (2000), all at the Rostov State University, Russia. Since 2006, he is a Professor of the Department of Physics at the Southern Federal University, Rostov-on-Don, Russia. His research interests include heterogeneous ferroelectrics, smart materials, domain and heterophase structures, and electromechanical effects in piezo-active composites. Author of five monographs, three edited conference proceedings, and over 400 papers, chapters in monographs, reviews, conference proceedings, and abstracts.

Christopher R. Bowen was born in Beddau, South Wales (UK) on January 18th, 1968. He earned a BSc (First Class) in Materials Science at the School of Materials, University of Bath, UK (1990) and worked on his DPhil thesis in the Department of Materials, University of Oxford, UK (PhD awarded in 1994). He joined the University of Bath, UK in 1998 and is now a Professor at the same University. His research interests are the manufacture and characterisation of ferroelectric ceramics and composites for sensor, actuator and energy-harvesting applications. He is author of three monographs, over 250 papers, chapters in monographs, conference proceedings, and abstracts.

Andrey V. Krivoruchko was born in Kharkiv (USSR, now Ukraine) on June 30th, 1984. He received the qualification "Engineer" (2006) at the Rostov State University, Russia, and degree "Candidate of Sciences (Physics and Mathematics)" (2009) at the Voronezh State University, Russia. Since 2010, he is an Associate Professor at the Don State Technical University, Rostov-on-Don, Russia. His research interests include electromechanical properties and orientation effects in modern piezocomposites and smart materials. Author of about 70 papers, chapters in monographs, conference proceedings, and abstracts.